P2.76 TWO NEW CONTRAIL DETECTION METHODS FOR THE COMPILATION OF A GLOBAL CLIMATOLOGY OF CONTRAIL OCCURRENCE

David P. Duda, Konstantin Khlopenkov
Science Systems and Applications, Inc. (SSA)), Hampton, Virginia

Patrick Minnis
NASA Langley Research Center, Hampton, Virginia

1. INTRODUCTION

One of the recommendations of the Federal Aviation Administration's (FAA) Aviation-Climate Change Research Initiative (ACCRI) is the development of a global climatology of linear contrail occurrence detectable via satellite remote sensing methods. Such a contrail climatology is necessary for the validation of a new generation of atmospheric models that represent contrail formation explicitly.

We present two new automated contrail detection algorithms (CDAs) that can be used to develop this climatology. These CDAs are part of a contrail climatology being developed by NASA Langley Research Center that includes concurrent contrail microphysical and radiative properties such as contrail optical depth, effective particle size and solar and broadband longwave radiative forcing that are derived using the CERES cloud detection and retrieval analyses (Minnis et al., 2008, 2009).

2. MODIFIED MANNSTEIN ET AL. CDA

The first algorithm is a modified version of the technique described by Mannstein et al. (1999), which detects linear contrails in multi-spectral thermal infrared (IR) satellite imagery using only two channels (11 & 12 μm) from the Advanced Very High Resolution Radiometer (AVHRR). This method requires only the brightness temperatures (BT) from the IR channels, with no other ancillary data, and can be applied to both day and night scenes. It uses a scene-invariant threshold to detect cloud edges produced by contrails, and 3 binary masks to determine if the detected linear features are truly contrails. However, these masks are not always sufficient to remove all non-edge features. To reduce the number of false positive detections due to lower cloud streets and surface features, we add observations from other IR radiance channels available on the MODerate-resolution Imaging Spectroradiometer (MODIS) on *Terra* and *Aqua*. The new modified method uses additional masks derived from the added thermal infrared channels to screen out linear cloud features that appear as contrails in the original method.

The modified CDA follows the same overall data flow as the original Mannstein et al. CDA. The IR brightness temperature measurements are first normalized to allow the data to be compared with scene-invariant thresholds. The brightness temperatures are first inverted to allow the BT and BTD data to be treated with the same procedures. (For example, T12.0 is the inverted BT for the 12.0 μm measurements.) Both the inverted BT and the brightness temperature difference (here, BTD1 is the BT difference between 10.8 and 12.0 μm measurements) data are then smoothed with a rotationally symmetric Gaussian 5×5 pixel lowpass kernel resulting in the images $\overline{T12.0}$ and $\overline{BTD1}$. The local standard deviation of the BT and BTD data are computed over the region of the Gauss kernel (for example,

$$\mathrm{STD}(12.0\ \mu\mathrm{m}) = \sqrt{\overline{(T12.0 - \overline{T12.0})^2}} \qquad (1)$$

by filtering the square of the differences between the original and smoothed images again with the same kernel. The difference between the original and the smoothed images was normalized with the local standard deviation to get the normalized image:

$$N12.0 = \frac{(T12.0 - \overline{T12.0})}{(\mathrm{STD}(12.0) + 0.1\ \mathrm{K})} \qquad (2)$$

where 0.1 K is added to the local standard deviation to limit the sensitivity of the normalization over very homogeneous regions. In addition to T12.0 and BTD1 used in the original CDA, the modified CDA also uses the following BT data:

Corresponding author address: David P. Duda, Science Systems and Applications, Inc., NASA Langley Research Center, Mail Stop 420, Hampton, VA 23681-2199; e-mail: david.p.duda@nasa.gov

T6.8 – water vapor channel (6.8 μm) BT
BTD2 = (T8.6 – T12.0),
BTD3 = (T8.6 – T13.3),
BTD4 = (BTD1 + BTD2).

The sum of the normalized images N=N12.0 + NBTD1 + NBTD2 was then convolved with a line filter of 19×19 pixels in 16 different directions, and the individual connected regions resulting from the filtering are considered as possible contrail objects. These objects are then checked against 6 binary masks to check for contrails. The first three masks are similar to the original CDA:

A. N = NBTD4 + NBTD2 + N6.8 + N12.0 + NBTD1 > 3.45 K.
B. BTD1 > 0.2 K.
C. Gradient(12.0 μm) < 2×STD(12.0 μm) + 1 K.

The threshold in condition A selects pixels having a higher-than-average normalized brightness, which is typical of thin cirrus in the BTD imagery. The relatively low BTD1 threshold was retained from the original CDA to allow detection of possible contrails over lower opaque clouds. Condition C compares the large-scale maximum gradient for 12.0 μm in a 15×15 pixel vicinity of a possible contrail pixel with the local standard deviation to eliminate features like coastlines which also appear as lines in the normalized 12.0 μm images.

Three additional binary masks are included in the modified CDA:

D. (Gr(6.8) – Gr(12.0)/(Gr(12.0) + 0.03) > -0.85.
E. NBTD3 > 0.0 K.
F. Gradient(BTD3) < 1.5×STD(BTD3) + 0.2 K.

All three masks are used to reduce the number of false positive detections of lower level cloud streets and other edge features in the IR imagery. Condition D compares the large-scale maximum gradient for the 6.8-μm water vapor channel with the gradient from the 12.0-μm channel. The water vapor channel tends to be smooth except in regions with high clouds, while the 12.0-μm channel shows cloudiness at all levels in the atmosphere. Thus, condition D removes regions where only low clouds are likely in the imagery. Condition E tends to mask regions with lower clouds more than areas with higher clouds, while condition F is similar in function to condition C.

Figure 1 shows an example of the modified CDA along with the original CDA and BTD1 image. The modifications in the contrail detection algorithm eliminate several false detections of contrails in the lower half of the imagery.

3. KHLOPENKOV CDA

The second algorithm is based primarily on image analysis and pattern recognition techniques. It uses the BTDs of the MODIS IR imagery producing the highest contrast for the contrails in a particular image (see Figure 2, left). The core of the algorithm consists of several stages of correlation analysis that use predefined linear patterns to match contrails with different widths and orientations. In the first stage, a 5×5-pixel masking is applied to a reduced image produced by the 2×2 box averaging of the original. This yields the directionality and strength of potential contrail fragments. Next, a more precise correlation with 16x16 patterns is applied to the original image, but only to the pixels with a high rating after the first stage and only with the patterns aligned closely to the directions detected at the first stage. Several patterns with different directions, widths, and subpixel offsets are tested to produce the highest correlation. The two-stage approach provides for high sensitivity to any linear features on the image while achieving a reasonable performance. The result from this correlation analysis is shown in Figure 2, right. The map of likely contrail nodes (pixels with high correlation) obtained from the initial analysis then undergoes a geometry analysis. At first, the nodes are checked to produce the optimal link pairs. The left-hand side of Fig. 3 shows the map by using different colors to indicate the different directions of the detected links. Based on the geometry of the linked pairs, the line segments are then generated with weights assigned according to the amount and weights of the included nodes. To discriminate contrails from common cirrus streamers, the algorithm analyses the density of the detected contrails that follow similar directions within a small area. The line segments that follow this local direction are assigned lower weights so that the algorithm suppresses the detected line segments that are likely to correspond to cirrus streamers.

Finally, the line segments are merged and extended by joining chains of links into lines, merging lines that are too close together, and extending lines by including weaker nodes too. Lines with low weight and limited length are discarded. The result is shown in Figure 3, right. The output contrail mask has different weights for each detected contrail indicating a combined confidence level of the detection. This allows some

flexibility for the end user when deciding whether a stricter or more liberal detection is needed.

Fig. 4 shows the final contrail mask and Fig. 5 shows the results from the modified Mannstein et al. CDA. Both methods show comparable contrail detections.

4. WAYPOINT DATA

Aircraft emissions data for 2006 (Wilkerson et al., 2010) were used to provide the location of commercial aircraft around the globe at 1-hour resolution. To provide a standard geographic grid for the contrail and aircraft data, all locations of the detected contrails and the commercial aircraft flight tracks derived from the waypoint data were re-gridded to a Lambert Azimuthal Equal-Area projection.

As a preliminary test of the new CDAs, the contrail masks produced by the modified Mannstein et al. algorithm have been compared to the global waypoint data provided by the FAA. The waypoint data have been used as a reference to distinguish thick diffused contrails from natural cirrus clouds. The bearings of the waypoint data-based flight tracks have been compared with the orientation of the detected contrails to determine which detected contrails are most likely false detections (Fig. 6). Future plans to improve the matching of detected contrails with waypoint data include using wind data from GEOS-4 [Goddard Earth Observing System (GEOS) Data Assimilation System – Version 4] analyses to advect the waypoint flight tracks and developing simple analytical models to simulate the growth and decay of contrails. These models will be superimposed on the advected waypoint flight tracks to determine the tracks that are most likely to match with the detected contrails.

The contrail detection masks developed from the CDAs form the first step in the contrail climatology process. The contrail masks will then be integrated into the NASA LaRC CERES cloud product retrieval system (Minnis et al., 2008, 2009) to derive contrail optical properties for a global contrail climatology. Figure 7 shows an example of contrail optical depth and longwave radiative forcing computed for a sample MODIS image.

5. SUMMARY AND FUTURE WORK

Two new contrail detection algorithms (CDAs) have been developed to detect linear persistent contrails from 1-km resolution thermal infrared imagery from MODIS. Both retrievals detect fewer but more reliable contrails than the original Mannstein et al. CDA. The Khlopenkov CDA is an independent contrail detection method that can be used as a check of the modified Mannstein algorithm. Additional datasets including flight track data from the ACCRI waypoint dataset are being used to improve the accuracy of the contrail detection algorithms. The CDAs form the first step in the development of a satellite-based contrail climatology of contrail occurrence and optical properties.

Future plans include the use of upper tropospheric wind data from GEOS-4 meteorological analyses to advect the flight tracks determined from ACCRI waypoint data. The advected flight tracks will be compared with contrail masks from the CDAs to determine conditions where false positive detections are likely. In addition, CERES cloud product retrieval information may also be used to reduce the number of false positive detections.

Efforts are currently underway to verify the accuracy of the modified Mannstein et al. CDA and to compile detection statistics of the CDA (including probability of detection, false alarm rate) by visual inspection of test cases. Once these tests are completed, we plan to process one year of *Aqua* and *Terra* MODIS imagery over Northern Hemisphere to create a contrail climatology, as well as a two-year contrail climatology over the contiguous United States (CONUS).

6. REFERENCES

Mannstein, H., R. Meyer, P. Wendling, 1999: Operational detection of contrails from NOAA-AVHRR data. — Int. J. Remote Sensing, 20, 1641-1660.

Minnis, P., and Co-authors, 2008: Cloud detection in non-polar regions for CERES using TRMM VIRS and Terra and Aqua MODIS data. IEEE Trans. Geosci. Remote Sens., 46, 3857-3884.

Minnis, P., and Co-authors, 2009: CERES Edition-2 cloud property retrievals using TRMM VIRS and Terra and Aqua MODIS data. IEEE Trans. Geosci. Remote Sens., submitted.

Wilkerson, J. T., M. Z. Jacobson, A. Malwitz, S. Baalsubramanian, R. Wayson, G. Fleming, A. D. Naiman, and S. K. Lele, 2010: Analysis of emission data from global commercial aviation: 2004 and 2006. *Atmos. Chem. Phys.*, **10**, 6391-6408.

Acknowledgements. This research is supported by the FAA ACCRI program, and by funding from the American Recovery and Reinvestment Act (ARRA).

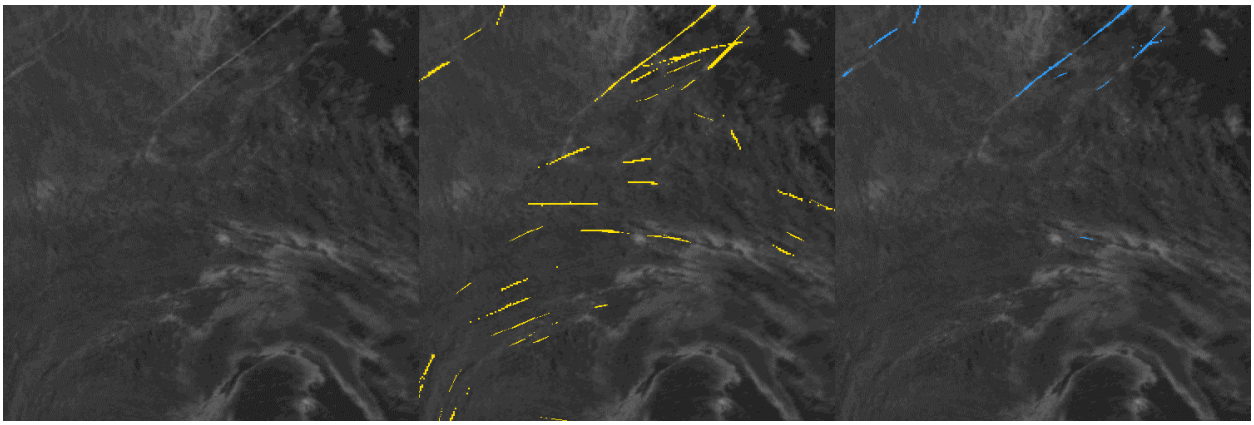

11 – 12 μm BTD Original CDA Modified CDA

Figure 1. *Terra* MODIS channel 31 (10.8 μm) minus channel 32 (12.0 μm) brightness temperature difference (BTD1) imagery over North Atlantic Ocean (1530 UTC 13 March 2006). Persistent contrails are visible in top part of imagery.

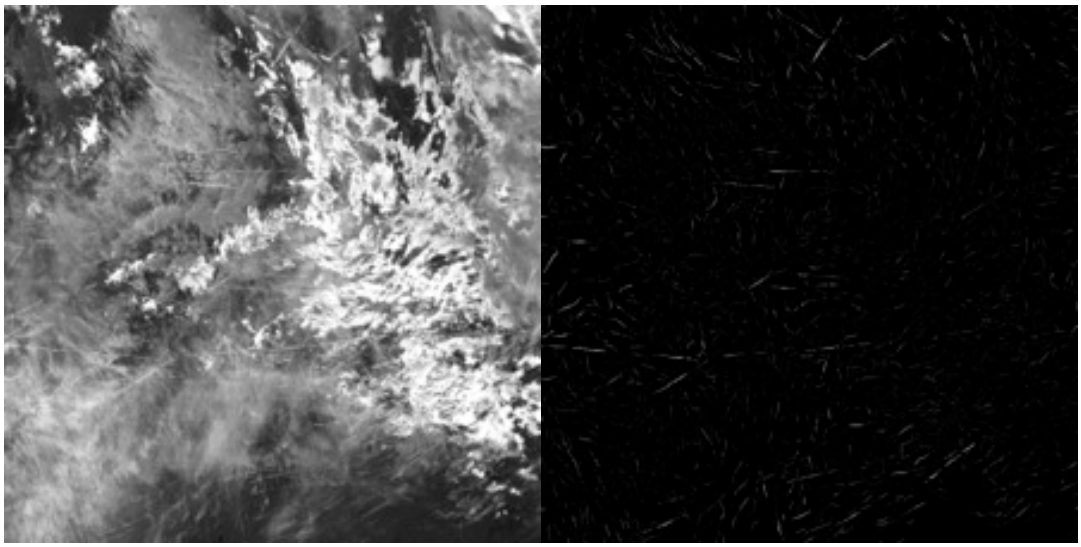

Figure 2. *Terra* MODIS channel 29 (8.6 μm) minus channel 32 (12.0 μm) brightness temperature difference (BTD2) imagery (left) and potential contrail fragments (nodes) determined from the correlation analysis (right).

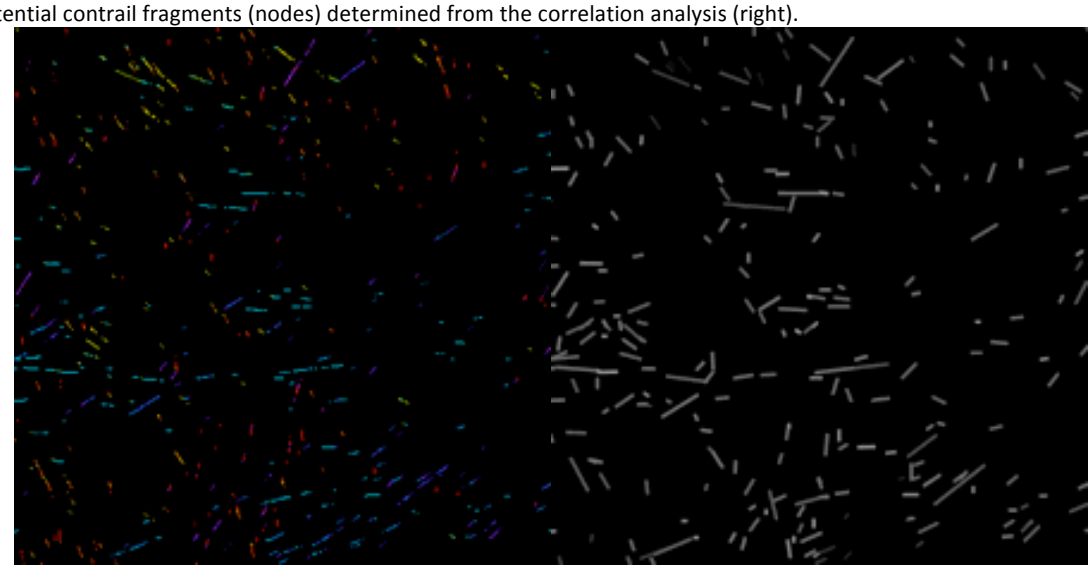

Figure 3. Map of optimal links between nodes coded by color to show different directions of detected links (left) and array of line segments obtained after merging and extending (right).

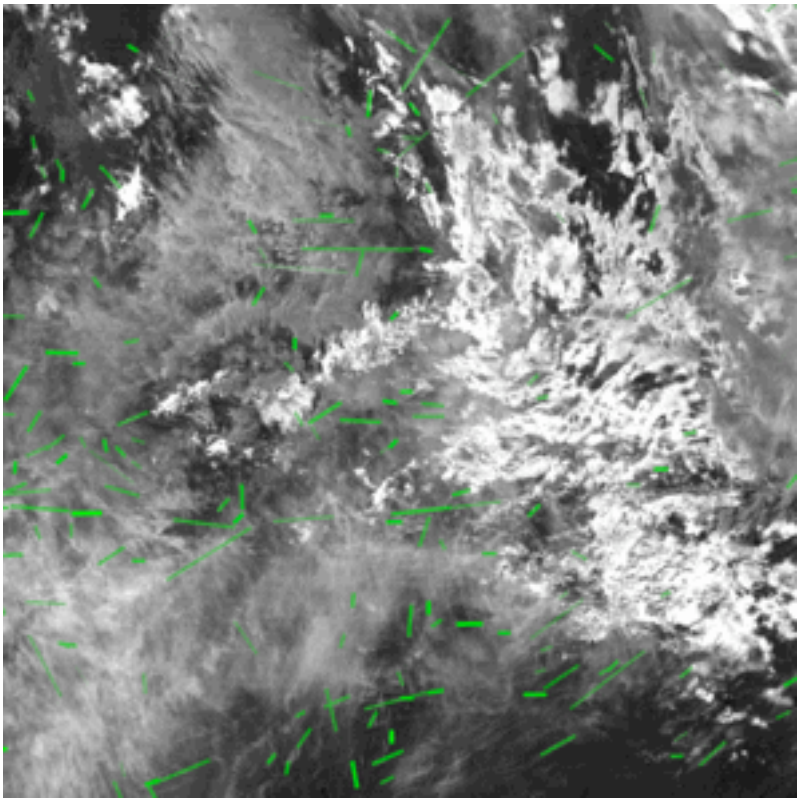

Figure 4. Khlopenkov CDA contrail mask (green lines) overlaid *Terra* MODIS BTD2 image.

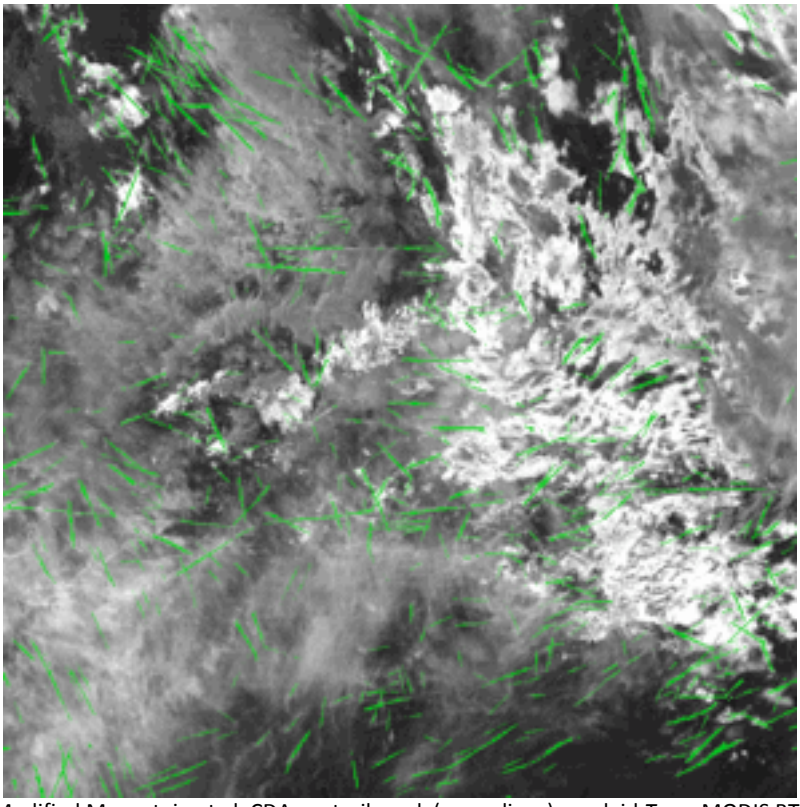

Figure 5. Modified Mannstein et al. CDA contrail mask (green lines) overlaid *Terra* MODIS BTD2 image.

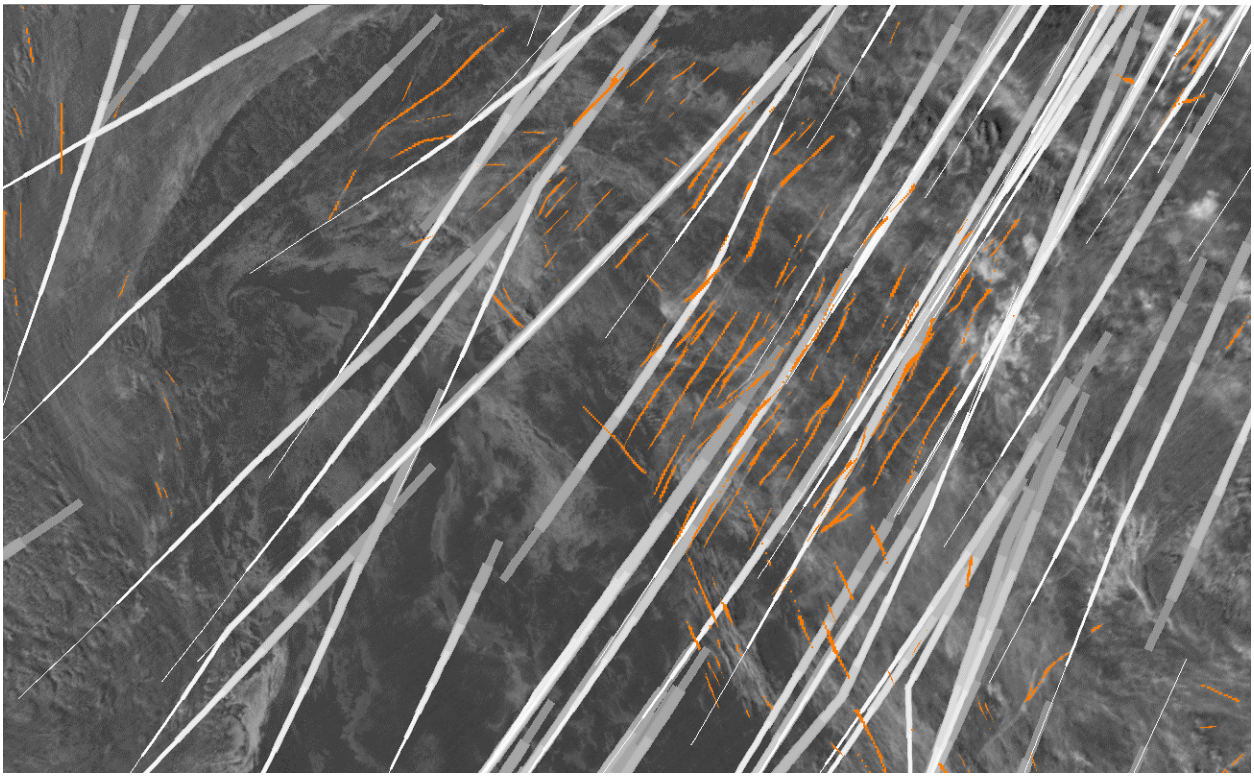

Figure 6. BTD1 image from *Terra* MODIS at 1345 UTC on 1 January 2006. Modified Mannstein et al. CDA contrail mask is overlaid in orange. Commercial jet flight tracks derived from ACCRI waypoint data appear as grey bands. The width and color of the flight tracks indicate their age relative to overpass time. Older tracks appear as darker and wider bands.

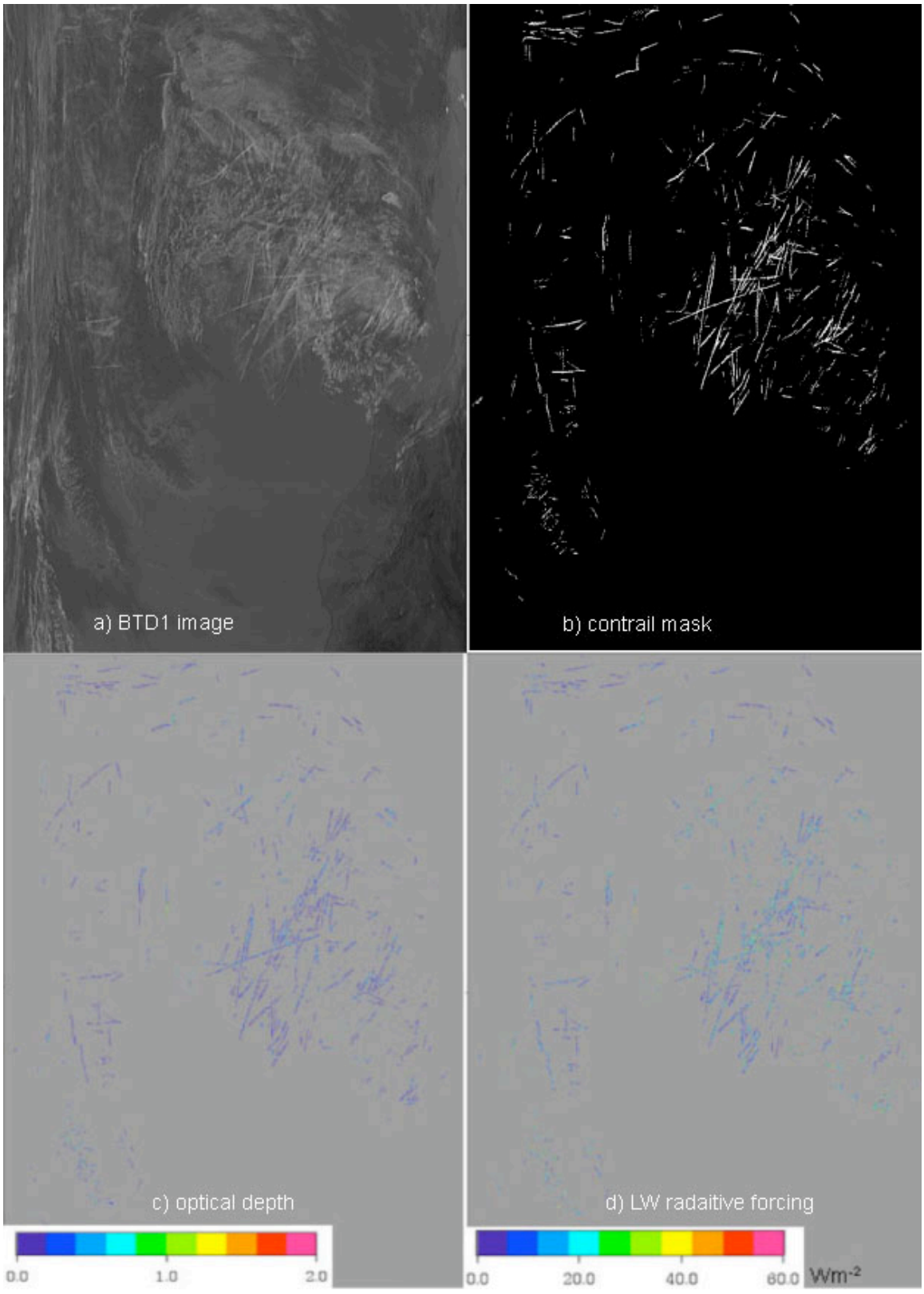

Figure 7. BTD1 image (A), contrail mask (B), contrail visible optical depth (C), and contrail longwave radiative forcing in W m^{-2} (D) computed for *Terra* MODIS image from 1135 UTC on 13 March 2006.